

A THERMAL AND MICROSTRUCTURE MODEL FOR LASER DEPOSITION OF Ti-6Al-4V

S. M. Kelly^{1,4}, S. S. Babu², S. A. David², T. Zacharia³, S.L. Kampe⁴

¹Joint Institute for Computational Sciences, Oak Ridge National Laboratory

²Metals and Ceramics Division, Oak Ridge National Laboratory

³Computing and Computational Sciences Directorate, Oak Ridge National Laboratory
P.O. Box 2008, Oak Ridge, TN 37831, USA

⁴Department of Materials Science and Engineering, Virginia Tech
213 Holden Hall, Blacksburg, VA 24061-0237 USA

Keywords: Ti-6Al-4V, laser deposition, thermal modeling, microstructure modeling

Abstract

Near-net shape processes, such as laser metal deposition (LMD), offer a unique combination of process flexibility, time savings, and reduced cost in producing titanium alloy components. The current challenge in processing titanium alloys using LMD methods is understanding the complex microstructural evolution as a part is fabricated layer by layer. The microstructure is affected by the repeated thermal cycling that occurs during the deposition process. The current work focuses on the thermal and microstructural modeling of multilayered Ti-6Al-4V deposits. Prior work with LMD-Ti-6Al-4V has shown that a complex microstructure evolves consisting of a two-phase alpha+beta structure. Depending on the location within the part, the Widmanstätten alpha may exhibit a colony (layer band) or basketweave morphology. A thermal model has been developed using finite difference techniques to predict the thermal history of LMD processes. The characteristics of a thermal cycle are used to qualitatively map the evolution of equilibrium and nonequilibrium phases in the deposit. The results of the thermal and microstructure models will be discussed in relation to the as-deposited microstructure.

Introduction

Laser metal deposition (LMD) processes have drawn much attention lately because of their ability to form small quantities of functional prototypes and structural parts at significantly reduced cost to the buyer.¹ Several commercialized LMD processes exist, including Laser Engineered Net Shaping (LENS*)², Directed Light Fabrication (DLF**)³, and Laser Additive Manufacturing (LAM***)⁴. All LMD processes are similar in that a three dimensional part in a CAD file is sliced into layers which in turn define laser scan trajectories. A high power laser is used to heat and melt metal powder, which solidifies to form a fully dense layer. The addition of multiple layers will produce a three dimensional fully dense part having a net or near-net shape. In the current work, Ti-6Al-4V (a common two-phase (HCP- α + BCC- β) heat-treatable titanium alloy) is deposited to form a near net shape single line build using the LAM process, which employs an 18 kW CO₂ laser and can deposit material at a rate of 0.9 to 4.5 kg hr⁻¹.

Microstructural evolution in laser metal deposited (LMD) Ti-6Al-4V has been demonstrated to be quite complex, with resultant microstructures consisting of large columnar prior beta grains, a basketweave Widmanstätten alpha morphology exhibiting a gradient in the individual alpha

* LENS is a trademark of Sandia National Labs and the US Department of Energy

** DLF is a trademark of Los Alamos National Labs and the US Department of Energy

*** LAM is a trademark of AeroMet Corporation, Eden Prairie, MN

lath width, and colony[†] Widmanstätten alpha or layer band morphology present in the build as illustrated in Figure 1 and Figure 2.^{5,6} Without knowledge of the thermal history developed during the build process, analysis of the resultant microstructure becomes difficult. Limited work^{5,7} has been performed to understand the microstructural evolution in LMD Ti-6Al-4V processes through thermal modeling.

A numerical model has been constructed to calculate the thermal history that develops as a result of the deposition of multiple layers of material in LMD processes.⁵ The focus of the current paper is to apply the thermal model to the LMD of Ti-6Al-4V and use the results to construct position-dependent microstructural “maps.” The maps will be based on known relationships among the thermal cycle characteristics and microstructural evolution. Presently, the resolution of the model is sufficient to allow one to predict the presence and location of a variety of microstructural features and forms, thus enabling comparisons with the observed microstructure.

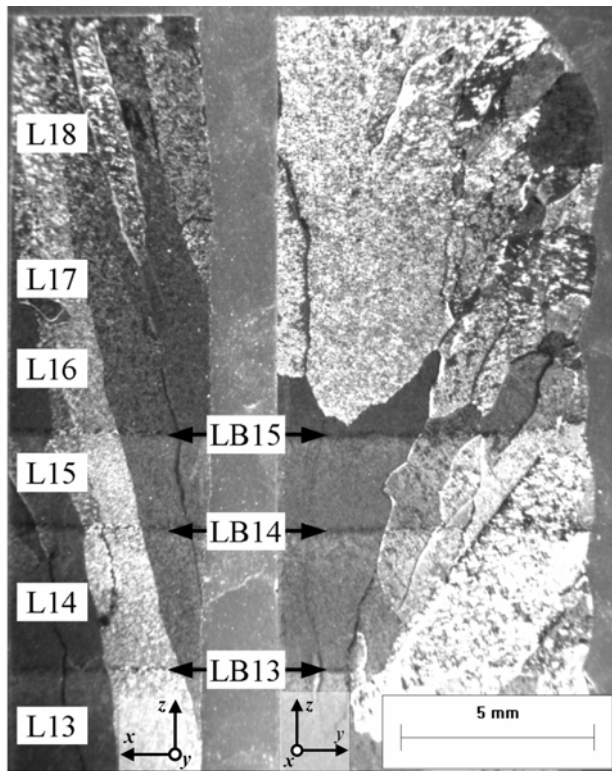


Figure 1: Macrostructure of LMD Ti-6Al-4V deposit showing the x-z (left) and y-z (right) section of the last 6 deposited layers in an 18 layer deposit. The laser travels in the x direction and additional layers are added in the z. Layers are indicated by “Ln” where n is the deposited layer and layer bands are indicated by “LBn”.

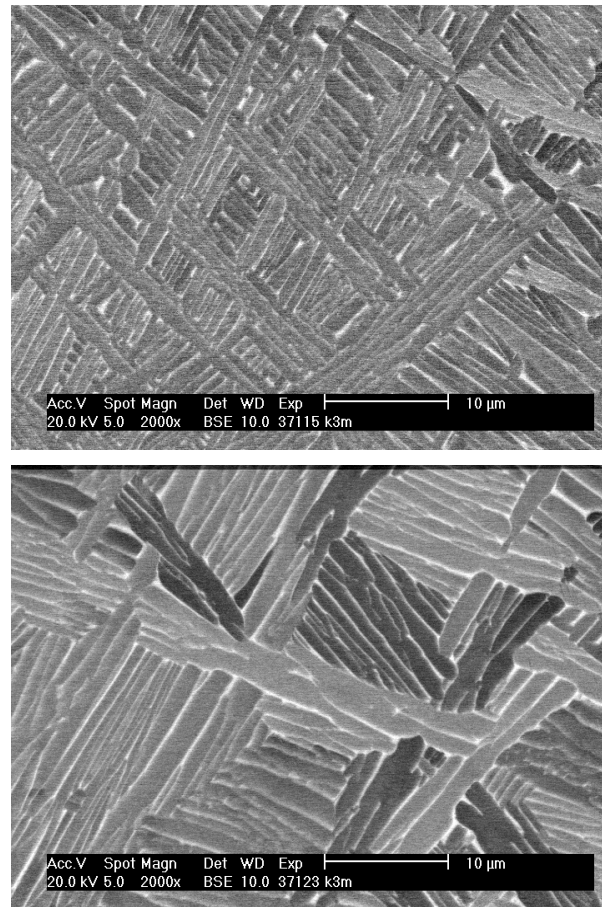


Figure 2: Backscattered electron micrographs of two regions within the deposit. Beta and alpha regions appear white and gray, respectively. Top shows a basketweave Widmanstätten alpha while the bottom shows a colony Widmanstätten alpha morphology that comprises the layer band.

Experiment

Thermal Model

The thermal model⁵ utilizes the two-dimensional implicit finite difference method⁸ to find a solution to the heat conduction equation at finite time steps during the course of the deposition process. An example of the computation domain and applied boundary conditions are

[†] A colony is defined as a several parallel alpha laths oriented in the same crystallographic direction

illustrated in Figure 3. Heat flow is assumed to occur in the y - z directions and not the x (direction of laser travel) which means the assumption is made that the temperature distribution is in a quasi-steady state in the x dimension, which is a common assumption known to produce good predictive accuracy. The additive nature of the LMD process is captured by adding a new layer to the computation domain after each pass of the heat source. The laser velocity, v_{laser} , and part length, l , are used to determine the frequency of layer addition. The node points (points where temperature is calculated) are distributed evenly within a layer and increased in size in the substrate for computational efficiency. Convective heat transfer due to the carrier gas (argon) used to deliver the metal powder to the deposit is assumed to occur on the outer surface of the substrate and deposit, and is defined by the heat transfer coefficient, h_{sub} and $h_{surface}$, and fluid temperature, $T_{\infty} = 310$ K. On the sides and bottom of the substrate, a fictitious heat transfer coefficient ($h_{sub} = 10^{10}$ W/m²K) is used to approximate a semi-infinite boundary condition. Symmetry of the deposit is utilized and as such, an adiabatic boundary condition is applied at all z positions corresponding to $y = 0$.

The laser heat source is modeled using a double ellipsoidal distribution of laser power that moves through the deposit with each time step, and can be calculated for any y , z , and time, according to Equation [1].⁹ A volumetric heat source was chosen over a surface heat flux because of the appreciable amount of melting that occurs during deposition. The parameters a , b , and c_i describe the semi-axes of the ellipsoid, specifically where the beam intensity falls to approximately 0.05 of the intensity at the center of the beam, which defines the variable $\sigma = 2.99$. The beam power delivered to the surface is $Q_{in} = P \cdot \alpha$, where P is the measured beam power and α is coupling efficiency of the beam and material. The heat source distribution is adjusted for the front ($i=1$) and rear ($i=2$) of the ellipsoid using the coefficient $f_i = c_i / (c_1 + c_2)$. Replacing z with $z - z_0$ in Equation [1] adds an additional parameter (z_0) that can be used to vary the penetration depth or focal point of the heat source. The heat source is applied to all nodes in the deposit, however, the energy input at distances greater than the semi-axes is minimal.

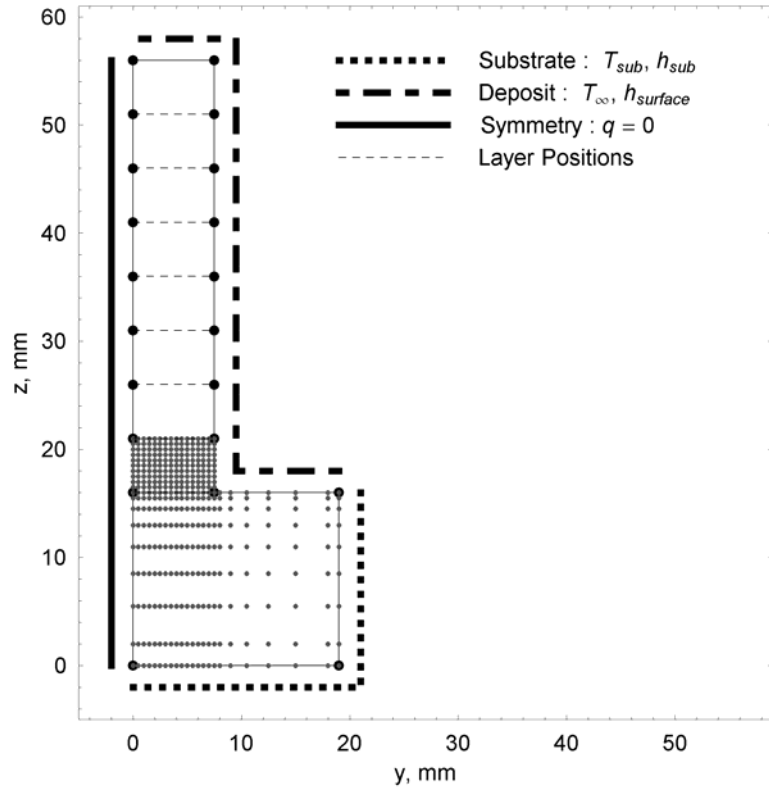


Figure 3: Schematic of the deposit geometry and locations of the surface boundary conditions. Node positions are shown for the substrate and first deposited layer.

$$Q(y, z, t) = \begin{cases} f_1 \frac{2\sigma\sqrt{\sigma}Q_{in}}{abc_1\pi^{3/2}} \exp\left(-\sigma\left(\frac{y^2}{a^2} + \frac{z^2}{b^2} + \frac{(c_1 - v_{laser}t)^2}{c_1^2}\right)\right) & t \leq c_1v_{laser} \\ f_2 \frac{2\sigma\sqrt{\sigma}Q_{in}}{abc_2\pi^{3/2}} \exp\left(-\sigma\left(\frac{y^2}{a^2} + \frac{z^2}{b^2} + \frac{(c_1 - v_{laser}t)^2}{c_2^2}\right)\right) & t > c_1v_{laser} \end{cases} \quad [1]$$

The thermal properties¹⁰ of Ti-6Al-4V are assumed to vary with temperature.

Unfortunately, the processing parameters for the as-deposited material under investigation are unknown; however, using estimates¹¹ of laser power and scan speed for LMD of Ti-6Al-4V and the dimensions of the deposit under investigation, it is possible to obtain parameters for Equation [1] that produce the measured microstructure characteristics in the deposit, specifically the dimensions of the heat affected zone (HAZ) and fusion zone(FZ). Table I shows fixed process parameters while Table II shows optimized parameters for Equation [1] that produce FZ and HAZ dimensions similar to those measured in the as-deposited material (from the center of the first deposited layer/substrate interface ($y = 0, z = 16$ mm)). The parameters contained in Table I and Table II will be used to generate the thermal data for an eight layer deposit that will be coupled with the microstructure model to determine microstructure evolution.

Table I: Constant processing parameters used in the thermal model.

Laser Power, P	Laser Velocity, v_{laser}	Part Length, l	T_{base}, T_{sub}	$h_{surface}$	h_{sub}	Layer: width x height	Substrate: width x height
13 kW	2.54 mm/s	250 mm	310 K	200 W/m ² K	10 ¹⁰ W/m ² K	15 x 5 mm	38 x 16 mm

Table II: Parameters used in Equation [1] to produce FZ and HAZ dimensions similar to those measured in the as received deposit⁶.

α	a, mm	b, mm	c_1 , mm	c_2 , mm	z_0 , mm	FZ Depth, mm (measured)	HAZ Depth, mm (measured)	FZ Width, mm (measured)	HAZ Width, mm (measured)
0.19	8.0	5.0	8.0	8.0	-1.0	2.69 (1.05 ± 0.22)	5.64 (4.48 ± 1.43)	7.505 (8.5 ± 1)	8.99 (9.5 ± 1)

Results

Thermal Model

The variation of temperature with time for positions at the top and bottom of the first (L1) and fifth (L5) layer deposited is shown in Figure 4. The calculations indicate that during the initial layer deposition, the entire layer sees temperatures well above the liquidus, before cooling to nearly room temperature. During the deposition of the second layer, nearly the entire first layer is remelted, while during the third layer deposition, only the very top of L1 is remelted. The most significant microstructural change is predicted to occur during the deposition of the fourth layer, where a region near the top of the layer experiences temperatures above the beta transus (1268 K), while the lower portion of the layer remains in the two phase region.

As for the deposition of the fifth layer (L5), shown in Figure 4, the peak temperatures and extent of remelting are similar to those described for L1, with the most noticeable difference being a reduction in the thermal gradient (dT/dz) at the peak temperatures. It is also observed that during the deposition of the fourth layer onto L5 (eighth layer on L1) that the top and bottom portions of L5 are heated into the single and two phase regions, respectively.

Table III shows ranges of calculated cooling rates for different z positions within the first layer. The cooling rates are calculated over the temperature range $\{T_{beta}, M_S\}$ or as near to the M_S as the thermal cycle will allow. During the deposition of the first two layers, we would expect a mixture of martensitic alpha (α') and massive alpha ($\alpha_{massive}$) to form because the calculated cooling rate is greater than the critical formation of these transformation products.¹² A mixture of diffusional and non equilibrium products would form during the third layer deposition, while thereafter only diffusional products would be expected.

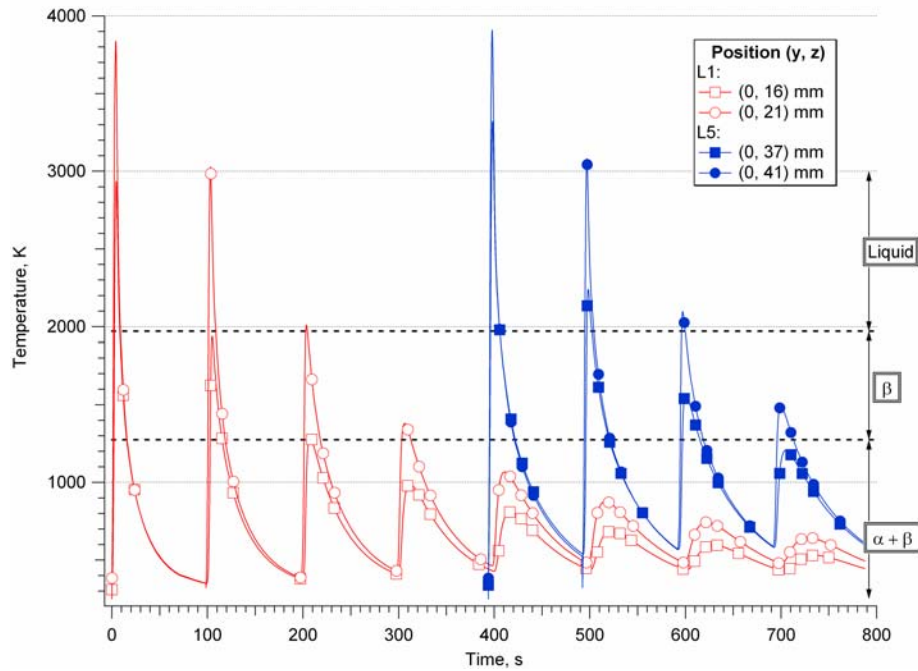


Figure 4: Temperature as a function of time for positions in the first (L1) and fifth (L5) layer along the centerline ($y = 0\text{mm}$) of the deposit. The lower and upper z positions correspond to the bottom and top of the layer. The symbols do not represent experimental data points, they appear for clarity.

Table III: Ranges of cooling rates calculated in the first layer for each layer added to the deposit.

Layer Deposition	1	2	3	4	5	6	7	8
Cooling Rate, K/s	36.7	26.9	21.1	16.5	9.06	4.44	3.43	2.54
	35.7	26.9	18.9	8.76	2.17	1.95	2.25	1.62

The z -position of the liquidus and beta transus are shown plotted versus a “time index” in Figure 5. A way to examine a portion of the thermal cycle time is by using the time index, calculated using the relationship: $TI = n + (t - (n-1) \cdot t_{pass}) / t_{range}$, where n is the pass number, t_{pass} the pass time, and t_{range} the time between major tick marks. Figure 5 shows the depth of melting and beta heating, as well as the length of the melt pool in the x direction along the centerline in the build since time is proportional to the x -direction. The depth of melting is nominally at least two layers ($>10\text{mm}$) and the length of the melt pool is nominally 26 mm, increasing from 18 to 28mm between the deposition of L1 and L8, respectively. The depth of equilibrium beta heating (z position where $T=T_{beta}$) increases from about 2.5 layers early in the process to 3.5 layers during the deposition of L8.

Qualitative Microstructure Map

The microstructural evolution is qualitatively mapped in Figure 6. Peak and minimum temperatures and cooling rates for each z position along the centerline ($y = 0$) combined with critical cooling rates¹² were used in combination with the criteria shown in Table IV to determine what and when morphologies would form. It is assumed from the equilibrium phase diagram that in order for the microstructure to change during a thermal cycle the peak temperature must be greater than $T_{eq} = 1020\text{K}$,¹³ which represents the temperature above which the equilibrium volume fraction of alpha begins to decrease. As subsequent layers are deposited, the peak temperature and existing morphology determine the resulting microstructure. If the peak temperature is greater than the beta transus Table IV still applies; however, if $T_{max} < T_{beta}$ and preexisting morphology is either α' or $\alpha' + \alpha_m$, then the preexisting morphology will be retained. For example, examine the deposition of layer 1 in Figure 6 where initially, the cooling rate is sufficient to produce a mixed $\alpha' + \alpha_m$ morphology in the first layer and a large portion of the substrate. When the second layer is deposited, the depth of heating

into the beta phase field is to the middle of substrate; therefore the $\alpha'+\alpha_m$ formed in the substrate during the initial deposition is retained (indicated by “L1”), while the region experiencing a temperature above the beta transus transforms to a mixed $\alpha'+\alpha_m$ morphology but the deposition of L2 is now responsible. In addition to showing what layer deposition causes a particular morphology, the depth of melting is indicated by a shaded region.

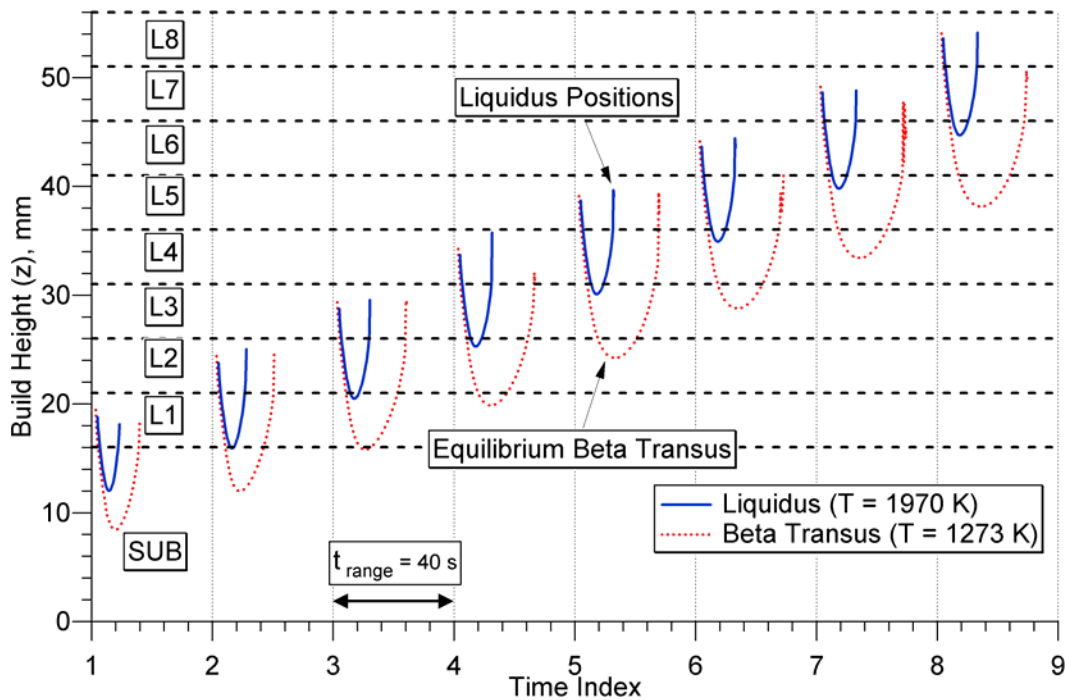


Figure 5: Iso-temperature curves for the liquidus ($T = 1970\text{ K}$), beta transus ($T = 1273\text{ K}$) for z positions along the centerline ($y = 0\text{ mm}$) of the deposit. The time axes (“time index”) has been adjusted to only plot the first 40 seconds of a laser pass, e.g. a Time Index = 1.5 yields a $t = 20$ seconds.

As multiple layers are added to the deposit, the map criteria predicts a transition from non-equilibrium (L1-L3) to equilibrium (L4-L8) products forming as a result of decreased cooling rates associated with a change in the geometry of the build. The majority of the deposit is predicted to contain diffusional transformation products, namely Widmanstätten $\alpha + \beta$, with a portion of L1 and the substrate retaining an $\alpha'+\alpha_{\text{massive}}$ morphology.

Discussion

It is evident from Figure 4, Table III, and Figure 6 that while the peak temperatures remain relatively constant during the deposition process, the cooling rates decrease as multiple layers are added. This is reflected in the qualitative microstructure map between the deposition of L3 and L4, where the morphology changes from a non-equilibrium to an equilibrium type. This is a result of the heat flow becoming increasingly one dimensional (and sluggish) as multiple layers are added. In addition, Figure 4 indicates that as multiple layers are added, the minimum temperature begins to increase, which in turn decreases the thermal gradients in the deposit. The change from two to essentially one dimensional heat transfer and minimum temperature that increases with each layer deposition necessitates a numerical as opposed to an analytical solution to the heat transfer problem.

It has been previously reported that the microstructural features present in laser deposited Ti-6Al-4V are a direct result of the thermal cycling^{7,14} experienced during the deposition process. It has been theorized⁶ that the graded basketweave Widmanstätten α morphology and colony Widmanstätten alpha or layer band morphology are formed in a layer n due to the deposition of layer $n+3$. During the $n+3$ deposition, a region near the top of layer n is heated completely into the beta phase field leading to a colony morphology, while the underlying material is heated

below the beta transus to a gradient in peak temperatures, producing a scale graded basketweave morphology. Heating above the beta transus results in a microstructure that is distinctly different from the underlying material. Upon further layer deposition, the peak temperatures experienced in layer n are insufficient to produce significant changes in the microstructure. The thermal model and microstructure map support the “ $n+3$ ” theory as shown in Figure 5 and Figure 6, where a narrow region of L5 ($38 < z < 41$ mm) experiences beta heating while the underlying material ($z < 38$ mm) remains below the beta transus. This sequence of super and sub beta transus heating is thought to lead to the layer band morphology and the probable location of the formation of a layer band during the deposition of L8 is indicated in Figure 6.

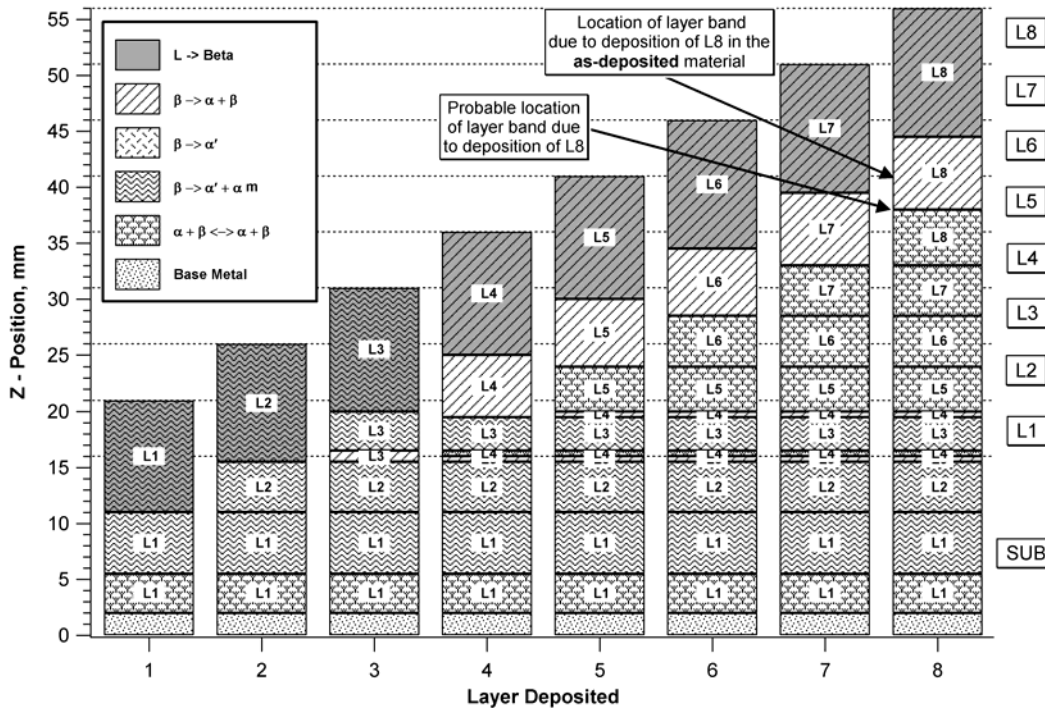


Figure 6: Qualitative microstructure evolution map for positions along the centerline ($y = 0$) of an eight layer deposit. The layer deposition responsible for a particular morphology is indicated by the label “ L_n ” where n is the layer being deposited. Horizontal gridlines designate the position of the layers in the deposit. Regions experiencing melting prior to another type of transformation (e.g. $L \rightarrow \beta \rightarrow \alpha + \beta$) are shaded gray.

Table IV: Morphology evolution criteria.

Peak Temperature	Minimum Temperature	Cooling Rate (K/s)	Resulting Morphology
$T_{\max} \geq T_{\beta}$	$T_{\min} < M_s$	$dT/dt > 410$	$\beta \rightarrow \alpha'$
		$410 > dT/dt \geq 25$	$\beta \rightarrow \alpha' + \alpha_m$
		$dT/dt < 25$	$\beta \rightarrow \beta + \alpha$
$T_{\beta} > T_{\max} > T_{eq}$	Any	$dT/dt < 25$, otherwise non-equilibrium (above)	Dissolution/Precipitation: $\beta + \alpha \leftrightarrow \beta + \alpha$
$T_{\max} < T_{eq}$	Any	Any	No Change, Base Metal

Cooling rates are from ¹²; T_{eq} is from ¹³.

The current microstructure map predicts the initial formation of non-equilibrium transformation products in the first few deposited layers, and thereafter equilibrium products are expected to form. The non-equilibrium products are eliminated (due to beta heating from subsequent layer additions) everywhere except in a portion of the substrate and L1, where they remain. Optical microscopy did not reveal any non-equilibrium products in the region where they are predicted to form. It should be noted that the calculated cooling rates where non-equilibrium products are predicted to form are only $10^\circ/s$ greater than the critical cooling rate for a diffusional

transformation; therefore, differences in the experimental and as-deposited conditions could result in variation of the critical cooling rates.

The results of the microstructure map indicate that using only peak temperatures and critical cooling rates to model the microstructure in this alloy may be too simplistic to produce detailed microstructure morphologies. In order to improve upon the existing model, the kinetics of the beta to alpha and alpha to beta phase transformations must be considered in order to fully capture the microstructure evolution of the deposit. Research efforts are currently focused in this area.

Conclusion

The results of the thermal support the theory that the layer deposition responsible for the formation the nominal (graded basketweave alpha) and layer band (colony alpha) morphologies in LMD Ti-6Al-4V are a result of the deposition of the $n+3$ layer onto layer n . The transition is a result of a region of layer n being heated into the beta phase field, while the underlying material remains in the two-phase regime.

A simple microstructure model has been developed based on peak temperatures and critical cooling rates is capable of predicting non-equilibrium and equilibrium beta transformation products in LMD Ti-6Al-4V deposits. The model predicts the formation of non-equilibrium transformation products in regions of the substrate and the first deposited layer, and equilibrium transformation products thereafter. The approximate position of the layer band morphology compares well will that seen in the as-deposited microstructure.

Acknowledgements

Research was sponsored by an appointment through the Joint Institute for Computational Sciences at the Oak Ridge National Laboratory. The Division of Materials Sciences and Engineering at the Oak Ridge National Laboratory sponsored a portion of this research. The Oak Ridge National Laboratory is operated by UT-Battelle, LLC for the U.S. Department of Energy under contract number DE-AC05-00OR22725. A portion of the research was sponsored through the Office of Naval Research under contract number N00014-98-3-0022 with Virginia Polytechnic Institute and State University.

Reference

- ¹ K. P. Cooper, JOM **53** (9), 29 (2001).
- ² M. L. Griffith, D. M. Keicher, C. L. Atwood et al., in *Proceedings of the Solid Freeform Fabrication Symposium* (University of Texas, Austin, 1996), pp. 125.
- ³ G. K. Lewis and E. Schlienger, Materials and Design **21**, 417 (2000).
- ⁴ F. G. Arcella and F. H. Froes, JOM **52** (5), 28 (2000).
- ⁵ S. M. Kelly and S. L. Kampe, "Microstructural Evolution in Laser-Deposited Multi-Layer Ti-6Al-4V Builds - Part I: Microstructural Characterization," Metallurgical and Materials Transactions A (accepted 12/2003).
- ⁶ S. M. Kelly, M.S. Thesis, Virginia Tech (<http://scholar.lib.vt.edu/theses/available/etd-05222002-223436/>), 2002.
- ⁷ P. A. Kobryn and S. L. Semiatin, JOM **53** (9), 40 (2001).
- ⁸ M. N. Özisik, *Finite Difference Methods in Heat Transfer*. (CRC, Ann Arbor, MI, 1997).
- ⁹ J. Goldak, A. Chakravarti, and M. Bibby, Metallurgical Transactions B **15B**, 299 (1984).
- ¹⁰ K. C. Mills, *Recommended values of thermophysical properties for selected commercial alloys*. (Woodhead, Cambridge, 2002).
- ¹¹ E. J. Whitney (Private Communication).
- ¹² T. Ahmed and H. J. Rack, Materials Science and Engineering A **243** (1-2), 206 (1998).
- ¹³ I. Katzarov, S. Malinov, and W. Sha, Metallurgical and Materials Transactions A **33** (4), 1027 (2002).
- ¹⁴ P. A. Kobryn, E. H. Moore, and S. L. Semiatin, Scripta Materialia **43** (4), 299 (2000); S. M. Kelly, S. L. Kampe, and C. R. Crowe, in *Solid Freeform and Additive Fabrication-2000*, edited by S. C. Danforth, D. Dimos, and F. B. Prinz (MATERIALS RESEARCH SOCIETY, Warrendale, 2000), Vol. 625, pp. 3.